frontiers | Frontiers in Materials

TYPE Review
PUBLISHED 28 September 2023
DOI 10.3389/fmats.2023.1236470

OPEN ACCESS

EDITED BY
Claudia Espro,
University of Messina, Italy

REVIEWED BY
Grant Henderson,
University of Toronto, Canada
Amey Rajendra Khanolkar,
Idaho National Laboratory (DOE),
United States

*CORRESPONDENCE
Charu Lata Dube,
charulata.dube@cug.ac.in

RECEIVED 08 June 2023
ACCEPTED 15 September 2023
PUBLISHED 28 September 2023

CITATION
Pilania RK and Dube CL (2023), Matrices for radioactive waste immobilization: a review.
Front. Mater. 10:1236470.
doi: 10.3389/fmats.2023.1236470

Matrices for radioactive waste immobilization: a review

Ritu Kumari Pilania and Charu Lata Dube*

School of Nano Sciences, Central University of Gujarat, Sector-30, Gandhinagar, Gujarat, India

Nuclear energy is considered a clean, reliable, and an inexhaustible energy source for power generation. Nuclear power is harnessed from nuclear fission reactions in a dedicated power plant. The by-products (produced in the nuclear power plant) are radioactive and pose a threat to the environment. The safe disposal of nuclear waste is vital to ensure the sustainable use of the nuclear energy. The immobilization of radioactive waste before final disposal is essential for the interim storage and transportation. This review summarizes the recent work on glass, ceramics, and glass–ceramics matrices to immobilize high-level waste. The synthesis methods, leaching behavior, and radiation resistance of matrices are discussed briefly.

KEYWORDS

glass, glass–ceramics, leaching, nuclear waste, radiation stability

1 Introduction

Primarily, nuclear energy is used in power generation, producing nearly 15% of electricity. Nuclear reactors (437 operational reactors in 2021 worldwide) produce more than 10% of all the energy consumed globally. Nuclear energy can fulfill the increasing demand of energy and contribute to reducing the consumption of fossil fuels and emission of greenhouse gases. Moreover, energy consumption in the future will rise, so the demand for building new nuclear power reactors to meet energy requirements will increase. Consequently, the generation of radioactive waste will be enhanced, owing to the increased use of fuel (uranium and plutonium oxide) to run the reactors (Englert et al., 2012). Radioactive waste is generated from chemical sludges, fission products, reactor decommissioning, and spent nuclear fuel; the radioactive waste or nuclear waste is generally categorized, based on its radioactivity level, as low-level waste (LLW), intermediate-level waste (ILW), and high-level waste (HLW), as summarized in Table 1 (IAEA Safety Standards, 2009).

The total radioactive waste comprises LLW, ILW, and HLW. HLW has the lowest volume in total radioactive waste and generates extensive heat due to radioactive decay. The reprocessed nuclear fuel constitutes the bulk of "high-level waste" (HLW), as defined by the International Atomic Energy Agency (IAEA) (McCloy and Goel, 2017). In order to reduce the amount of radionuclides in the spent nuclear fuel, efforts are being made to extract Pu and U using the PUREX process. The PUREX process is a liquid–liquid separation process that utilizes tri-n-butyl phosphate (TBP). In addition, normal paraffinic hydrocarbon (NPH) and numerous solvents are used (Baumgärtner and Ertel, 1980; Herbst et al., 2011). TBP is used for selective extraction of Pu and U from spent nuclear fuel. The modern PUREX processes include more than two cycles of extraction, scrubbing, and striping the fuel (Kumari et al., 2020). The extracted Pu and U from the spent nuclear fuel can be reused after enrichment and conditioning. Later, the resulting waste obtained after reprocessing the spent fuel can be immobilized in a matrix, followed by final disposal in the deep geological

TABLE 1 Classification of radioactive waste and their sources.

Nuclear waste type	Volume in total waste (in %)	Radioactivity percentage of total nuclear waste (in %)	Source
LLW	90	1	Paper, clothing, tools, and rags from industries, hospitals, and nuclear fuel cycles
ILW	7	4	Contaminated materials from reactor decommissioning, resins, chemical sludges, and metal fuel cladding
HLW	3	95	Fission products, transuranic elements, and minor actinides from burning of uranium fuel in the nuclear reactor and from hospitals

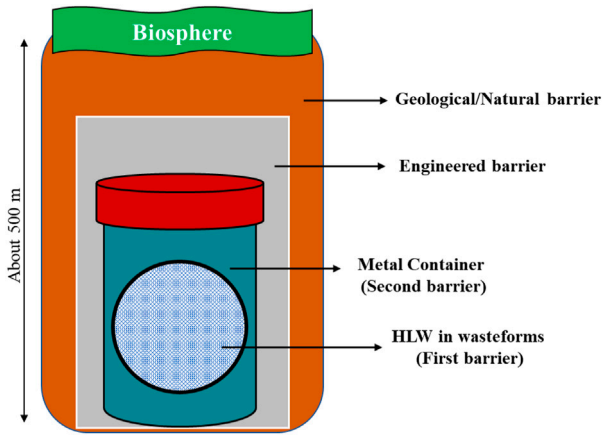

FIGURE 1
Multi-barrier system of HLW disposal.

repository. Invariably, the radioactive waste generated from nuclear power plants is chemically complex and contains a wide range of fission products (Lee et al., 2006; Lee et al., 2013a; Jantzen et al., 2013). In addition to the spent nuclear fuel, legacy waste (generated during the Second World War and decommissioning of a nuclear site or reactor) comes under the category of HLW (Zorpette, 1996; Rao, 2001; Beckitt, 2012).

Depending upon the category of radioactive waste, the disposal of wastes can be carried out in landfill disposal, shallow-level disposal, and deep geological repositories (Darda et al., 2021). HLW is further categorized as i) long-lived radionuclides and ii) short-lived radionuclides. The half-life time of long-lived radionuclides, such as ^{239}Pu, ^{129}I, ^{99}Tc, and ^{93}Zr, is of the order of millions of years. On the other hand, the half-life time of short-lived radionuclides, such as ^{90}Sr, ^{137}Cs, ^{60}Co, and ^{192}Ir, is hundreds to thousands of years (IAEA, 2017; Ojovan et al., 2019; Ojovan, 2023). Long-lived radionuclides containing HLW are proposed to be disposed using the concept of a multi-barrier system (as shown in Figure 1). The multi-barrier system has different layers of barriers. The first barrier is wasteform; the second barrier is the HLW container; the third barrier is an engineered barrier; and the fourth is a geological barrier (Lee et al., 2006; Jantzen and Ojovan, 2019).

HLW is immobilized in a suitable wasteform before disposal in the multi-barrier system. Immobilization is the process where the waste is made immovable in the form of wasteforms through various routes, such as containment, solidification, and vitrification (Jantzen et al., 2013; Li et al., 2021; Jo et al., 2022). The containment process includes pumping, capping, and installation of slurry walls. The solidification process involves the transformation of waste into a stable and immovable form for storage or disposal, such as cementation. The vitrification process transforms hazardous waste into a chemically stable wasteform, such as glass, glass–ceramic, and ceramics (Meegoda et al., 2003).

The chemical durability and radiation stability of matrix/wasteforms of any chosen wasteform should be good for immobilizing waste radionuclides (Lee et al., 2006). The wasteforms for immobilization of HLW are primarily of three types i) glass, ii) ceramic, and iii) glass–ceramic wasteforms. A potential wasteform/matrix should have the following features (Wang and Liang, 2012; Lee et al., 2013a; Ojovan and Lee, 2014; Hyatt and Ojovan, 2019; Jantzen and Ojovan, 2019).

1) The loading capacity (ability to accommodate waste inside the matrix) should be high. In addition, the wasteform should be able to incorporate daughter products as well.
2) The wasteforms should have good durability under aqueous conditions. The waste must always be isolated from the biosphere until the radionuclide becomes non-radioactive (10 half-lives) (Khan et al., 2010). The porosity of the matrix should be negligible as minimal porosity will help avoid permeability and hence leachability under aqueous conditions.
3) The matrix should be highly radiation-tolerant to sustain under the α- and β-decays of radionuclides against any phase changes, owing to the heat generated during the decay processes inside the matrix.
4) The volume of wasteforms should be as small as possible. It should have good mechanical properties, which will be helpful in avoiding fracture or crack during transportation and handling.
5) The composition of wasteforms should be close to natural analogs. However, there is no true natural analog for borosilicate glass wasteform as it includes a high content of boron and radionuclides. However, natural basaltic glass can be considered a natural analog of borosilicate glass because of its chemically durable properties (Techer et al., 2001; Crovisier et al., 2003).

The different types of wasteforms are discussed in the following subsection.

2 Types of wasteforms

2.1 Non-crystalline wasteforms

Glass is an inorganic solid prepared by quenching from the melt while preventing the crystallization. The typical glass structure has mainly three constituents, namely, 1) network formers, 2) intermediates, and 3) network modifiers (Lee et al., 2006; Lee et al., 2013b; Hyatt and Ojovan, 2019). The open and random structure of glass is primarily responsible for achieving high waste loading and chemical durability (Jantzen, 2011). The radionuclides in glass are immobilized by primary or/and secondary bonding within the glass network. The glass has a random structure with specific characteristics as per the model proposed by Zachariasan (Varshneya and Mauro, 2019; Shelby, 2020). The characteristics are i) no oxygen atom may be linked to more than two cations; ii) the cation coordination number should be 3 or 4; iii) the oxygen polyhedra should share corners only (not edges or faces); and iv) for a 3D network, at least three corners must be shared. Glass has been considered for immobilizing matrix due to its structural flexibility, simple synthesis route, high waste loading capacity, and inexpensive raw materials. The glass wasteforms have good radiation stability. The high chemical durability enables the glass to remain stable in corrosive environments for thousands of years (Kavaz et al., 2020).

2.2 Crystalline wasteforms

The ceramic wasteforms have widely been divided into a) single-phase ceramics, such as zircon, to accommodate a limited range of active species, such as Pu; and b) multi-phase systems, such as Synroc (composed of hollandite ($BaAl_2Ti_6O_{16}$), zirconolite ($CaZrTi_2O_7$), and perovskite ($CaTiO_3$)), to accommodate a wide range of active species (Ringwood et al., 1979; Ojovan et al., 2019; Orlova et al., 2019). However, Synroc has its own disadvantages, such as being thermodynamically unstable (Nesbitt et al., 1981). Synroc is not being used for immobilization of HLW by any country to the best of our knowledge. Furthermore, the pyrochlore-structured titanate/zirconate ceramics, such as $Gd_2Zr_2O_7$ and $Er_2Zr_2O_7$, are potential ceramic wasteforms (Maddrell, 2001; Ewing et al., 2004; Sattonnay et al., 2008). Zirconolite is mainly used to immobilize the long-lived radionuclides (Pu), while the perovskite phase is primarily suitable for the short-lived radionuclides (Sr and Ba). The hollandite phase is a potential candidate to immobilizing Cs, K, Rb, and Ba radionuclides (Ringwood, 1978; Xu and Wang, 2000). The major disadvantage of crystalline wasteforms is their inability to accommodate a wide range of radionuclides (Wang and Liang, 2012).

2.3 Glass–ceramic wasteforms

Recently, the glass–ceramic materials (GCMs) with mineral-like phases are reported for the immobilization of complex waste (Ojovan et al., 2021). The major component of GCM may be either the crystalline phases with the glass acting as a binding agent or the vitreous phase with the crystalline particles dispersed in the glass matrix (Ojovan et al., 2008; Donald, 2010; Ojovan et al., 2021). The most exciting feature of GCMs is that both the long-lived and short-lived radionuclides can be immobilized. The long-lived radionuclides can be immobilized in stable and durable crystals, whereas the short-lived radionuclides can be immobilized in the vitreous phase. The advantages of immobilizing complex HLW in GCMs are as follows: a) GCMs have nearly zero porosity and hence lead to minimal leaching. It can be synthesized on a mass scale by existing glass-forming techniques; b) the desired glass and ceramic can be incorporated in a single matrix (Zanotto, 2010).

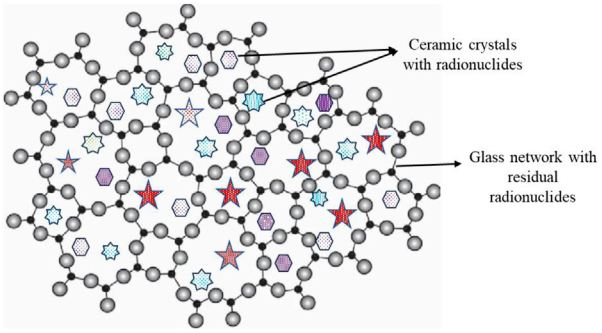

FIGURE 2
Schematic representation of glass–ceramic wasteforms.

Glass–ceramic wasteforms possess higher durability, high thermal stability, and superior mechanical properties than glass and ceramic wasteforms (Davis and Zanotto, 2017). The ceramic crystals are embedded in a glass network of the glass–ceramic matrix, as shown in Figure 2.

The leaching of radionuclides will be initially hindered by the glass phase surrounding the ceramic phase. Hence, the glass is another barrier to the outgoing movement of radionuclides from the ceramic phase. The highly durable crystals homogeneously dispersed in the bulk of the glass matrix will form an enhanced containment barrier for radionuclides. There is a potential risk that conventional glass wasteforms partially crystallize during cooling or because of radiation effects over long periods, especially in HLWs (Mahmoudysepehr and Marghussian, 2009). The glass–ceramic wasteforms are chemically more flexible and less expensive to prepare than pure ceramics, and in addition, they offer higher chemical durability than conventional glass and ceramic wasteforms. The different wasteforms, their suitability, and composition are tabulated in Table 2.

3 Synthesis of wasteforms

Wasteforms can be synthesized by different methods, rendering different properties. The wasteforms are invariably synthesized by employing the melt-quench, solid-state sintering, hot pressing, microwave sintering (Wei et al., 2020), self-propagating high-temperature synthesis (SHS) (Barinova et al., 2008), and spark plasma sintering (SPS) methods (Aldean et al., 2022). The synthesis method should be simple, cost-effective, and capable of avoiding the production of secondary radioactive waste. The synthesis temperature should be low so that evaporation of volatile radionuclides (such as I, Cs, and Ru) can be minimized. The viscosity of the molten glass should be optimum so that

TABLE 2 Different types of wasteforms and their composition.

Wasteform	Composition	Country	Waste type	Reference
Magnox	$47.2SiO_2$-$16.9B_2O_3$-$4.8Al_2O_3$-5.3MgO-$8.4Na_2O$-17.4Others	UK	HLW	Backhouse et al. (2019)
R7T7	$45.5SiO_2$-$14B_2O_3$-$4.9Al_2O_3$-$9.9Na_2O$-$2.9Fe_2O_3$-22.8Others	France	HLW	Gin et al. (2011)
K26	$48.2SiO_2$-$7.5B_2O_3$-$2.5Al_2O_3$-$16.1Na_2O$-15.5CaO-10.2Others	Russia	LILW	Ojovan et al. (2005)
CCM	$52P_2O_5$-$19Al_2O_3$-$21Na_2O$-7.8Others	Russia	HLW	Ojovan and Batyukhnova (2019)
DWPF	$50SiO_2$-$8B_2O_3$-$4Al_2O_3$-$8.7Na_2O$-1.4 MgO-27.9Others	United States	HLW	Ojovan and Batyukhnova (2019)
PAMELA	$52.7SiO_2$-$13.2B_2O_3$-$2.7Al_2O_3$-$5.9Na_2O$-4.6CaO-20.9Others	Germany–Belgium	HLW	Ojovan and Batyukhnova (2019)

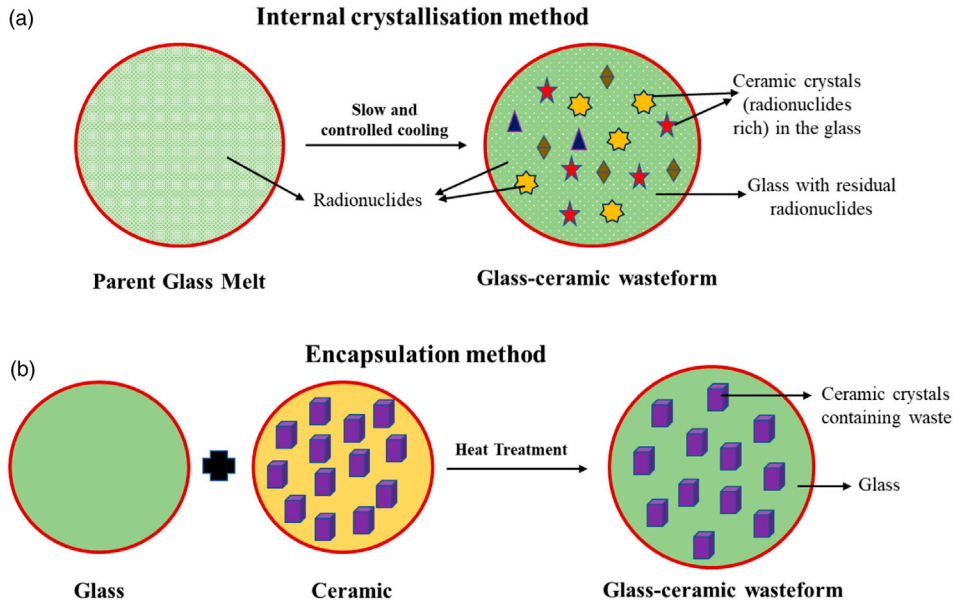

FIGURE 3
Schematic representation of glass–ceramic wasteform synthesis. **(A)** Internal crystallization and **(B)** encapsulation method.

homogenization and pouring can be achieved. The following subsections briefly describe a few selected conventional and modern methods for the synthesis of wasteforms.

3.1 Melt-quench method

In this method, oxide/carbonates/nitrates of parent materials are mixed and heated in a crucible to a desired temperature to get a molten liquid (melt). To get homogeneity, the melt is continuously stirred. When the melt is quenched (non-equilibrium cooling), it produces a glass structure. The traditional method is preferred because it is simple and efficient even at the mass-scale production.

3.2 Internal crystallization and encapsulation method

The glass–ceramic can be synthesized under slow and controlled molten liquid cooling conditions by employing the internal crystallization method. Under controlled cooling, nucleation occurs, and growth of crystals takes place in the glass matrix. The method results in the formation of crystals inside the glass structure (Rawlings et al., 2006; Zhang et al., 2022). The thermal stability of these glass–ceramic wasteforms is relatively high compared to the glass and ceramic wasteforms (McCloy and Goel, 2017).

In the encapsulation method, the ceramic phase is added directly to the glass charge. The powder-containing glass charge and ceramic are invariably maintained at the melting temperature of the glass. Subsequently, the homogeneous melt is quenched, and the glass-ceramic wasteform is obtained. The schematic representation of both the methods for the synthesis of glass–ceramic wasteforms is shown in Figure 3.

3.3 Sintering Methods

The ceramic wasteforms can be synthesized using conventional solid-state sintering, hot pressing, and the most recent microwave

sintering methods. In recent days, the wasteform synthesis through microwave energy is a novel concept. The microwave (MW) heating method can be employed to synthesize different wasteforms to minimize melting time/temperature and thereby power consumption. MW heating is rapid and volumetric in nature (Knox and Copley, 1997). The heating of materials under microwaves depends upon materials' dielectric and magnetic properties. Most of the oxide precursors are poor microwave absorbers at room temperature. Nevertheless, above a critical temperature, oxides start absorbing microwaves (Mandal and Sen, 2015). In a non-absorbing system, initially, oxides are raised to a critical temperature with the help of a microwave susceptor (SiC) (Mandal and Sen, 2017).

4 Immobilization mechanism

The wasteforms discussed in the previous section can be utilized for immobilization of HLW mainly using two concepts (Donald et al., 1997; Ojovan and Lee, 2014):

(A) Waste dissolution: the waste can be incorporated into the glass or crystalline (single or multiphase) phase. The radionuclides are immobilized at a microscopic scale in the wasteforms (National Research Council, 2011).

(B) Waste encapsulation: the wasteforms can be envisaged, where a high loading of radionuclides can be encapsulated in a durable glass/ceramic/glass–ceramic phase. This method mainly immobilizes radionuclides at a microscopic scale. If the resultant matrix (obtained after incorporating radionuclides) exhibits good chemical durability, the matrix can be considered a secondary barrier against dissolution through water (Donald et al., 1997). The inclusion of foreign atoms in the random glass network can improve the stability and durability of the matrix. The foreign atoms may settle into interstitial/substitutional sites of the crystal structure of ceramic wasteforms. In a glass–ceramic wasteform, foreign atoms may settle either in the random glass network or at interstitial/substitutional sites in the ceramic phase. The chemical durability and radiation stability of the wasteform play important roles in the selection of wasteforms. The chemical durability and radiation stability of different kinds of wasteforms are discussed in the following subsections.

5 Chemical durability of wasteforms

The chemical durability of the matrix defines the long-term structural integrity and the elemental release from the matrix (Ojovan and Lee, 2014; Clark et al., 2021). The standard protocols are employed to study the leaching behavior of the immobilizing matrix. The frequently used protocols are described as follows (Strachan et al., 1982; Thorpe et al., 2021):

i) Material characterization center (MCC-1): the leach test setup is static in nature, and the test is performed at temperatures <100°C. The reference temperatures are taken as 40°C, 70°C, and 90°C. The glass monolith is immersed in de-ionized water (DI) water/reference groundwater at the reference temperatures. The sample surface area to water volume (SA/V) ratio is usually maintained as low as ~10 m^{-1}. The test duration is generally 28 days, but it can vary. The test is used to measure the initial rate and residual rates, and to understand the mechanism of alteration layer formation.

ii) Material characterization center (MCC-2): the static leach test is performed in the temperature range 100°C–200°C. The reference temperatures are taken as 100°C, 150°C, and 190°C. The glass monolith is immersed in DI water/reference groundwater for a duration of 28 days. The test is used for the analysis of the residual rate and alteration layer.

iii) Material characterization center (MCC-3): this test is performed on powdered specimens. The powdered specimens are kept under a constant agitation condition. The sample surface area to water volume (SA/V) ratio is maintained as high as 2000 m^{-1}. The test temperature and duration are similar to the MCC-2 test. This test gives information related to the residual rate of leaching.

iv) Material characterization center (MCC-4): the additional parameter of the leachant flow is introduced in the test. The reference flow rates used are between 0.1 and 0.001 mL min^{-1}. The glass monolith is used for the test and performed at temperatures <100 °C for 28 days. This test is suitable to measure the initial rate of leaching.

v) Material characterization center (MCC-5): the glass monolith is kept in the flowing leachant. The leaching solution is DI water, and the test temperature ranges between 35°C and 300°C. The test is used to measure the initial rate of leaching in distilled water only.

vi) Product consistency test (PCT-A): this is a static leach test and performed at 90°C. The powdered sample (74–149 μm) is kept in DI water for 7 days. The sample surface area to water volume (SA/V) ratio is maintained as high as 2,000 m^{-1}. The test is performed to measure the initial rate of leaching.

vii) Product consistency test (PCT-B): this test is similar to PCT-A. The sample powder is kept at temperatures <100°C. The test is used to measure the initial rate and residual rates of leaching.

viii) Vapor hydration test (VHT): the leach test is performed with a glass monolith sample in the temperature ranges 5°C–300°C. This test is static in nature and performed under steam for 24 days. The residual rate and alteration layer thickness are measured.

ix) Single-pass flow-through test (SPFT): the test is performed with glass powder or monoliths at temperatures <100°C. This is a dynamic test, and the forward rate of leaching/dissolution is generally measured.

6 Leaching mechanism of the wasteforms

The leaching of the matrix generally happens in three stages:

Stage (1): **hydrolysis of network:** in this process, ion exchange reactions take place between the matrix (glass, ceramic, or glass–ceramic type network) and the aqueous media; as a result, the ion exchange reactions (hydrolysis of the matrix) occur (Bunker et al., 1984; Abrajano et al., 1986; Clark et al., 1992).

Stage (2): **network dissolution:** in this process, breakage of bridging bonds occurs and secondary phases (possible phases: analcime, phillipsite, sepiolite, and tobermorite) get precipitated. In this process, dissolution can decrease or increase depending on the type of phases on the matrix surface (Pierce et al., 2010; Corkhill et al., 2013).

Stage (3): **formation of the hydrated gel layer:** the dissolution rate is related to the formation of a gel layer/alteration products (zeolites and calcium silicates). The amorphous gel layer's composition and thickness depend upon the matrix composition, temperature, and pH of the aqueous media. The alteration products are crystalline, sandwiched between the hydrated gel layer and the aqueous media. This process plays a crucial role in the leaching of the matrix as it will alter the thickness of the hydrated gel layer (Ma et al., 2017; Hopf et al., 2018; Wilkinson et al., 2019; Gin et al., 2020; Stone-Weiss et al., 2020; Zubekhina et al., 2020).

The normalized leach rate ($g.m^{-2}.day^{-1}$) of nuclide i from the matrix can be calculated using the following expression (Ojovan et al., 2019):

$$NR_i = \frac{C_i}{f_i.\,(SA/V).t}. \quad (1)$$

Here, C_i: concentration of element "i" in the solution ($g\ L^{-1}$);
f_i: mass fraction of element "i" in the samples (unitless);
SA: surface area of the sample (m^2);
V: leachant volume (L) and t is the leaching time.

6.1 Chemical durability of glass wasteforms

In order to investigate the chemical durability of wasteforms, the United Kingdom HLW glass was synthesized with 25 wt% of simulated high-level waste (Corkhill et al., 2013). The chemical durability of glass was studied at pH 12.7 in a saturated $Ca(OH)_2$ solution and alkaline water at pH 9.8. The dissolution of elements was explained in three regimes that were named as the i) initial incubation phase, ii) intermediate phase, and iii) residual phase. The normalized dissolution rates of glass powder (S/V: 10,000 m^{-1}) for elements B, Li, Na, and Si were found to be 1.9×10^{-5}, 1.7×10^{-5}, 4.5×10^{-5}, and 4.2×10^{-7} g $m^{-2}day^{-}1$ after 168 days, respectively, in alkaline water, which was nearly an order lower than obtained rates of 28 days. The normalized dissolution rates of glass powder in a saturated calcium hydroxide solution of B, Li, Na, and Si were found to be of the order of 10^{-5} g $m^{-2}day^{-1}$ after 168 days, respectively; C–S–H ($CaO–SiO_2–H_2O$) phase formation was observed in the initial incubation phase, which led to the reduction in dissolution rates. The normalized dissolution rates of glass monolith samples (S/V: 10 m^{-1}) in the saturated $Ca(OH)_2$ solution of B, Li, and Na were obtained as 5.4×10^{-5}, 1.8×10^{-4}, and 3.6×10^{-4} g $m^{-2}.day^{-1}$ after 70 days, respectively. The leaching of Si was not observed throughout the period in glass monolith samples. The same group investigated the long-term leaching behavior of International Simple Glass (ISG) in acidic to hyper alkaline conditions using PCT and MCC-1 leaching tests for 120 and 720 days, respectively (Backhouse et al., 2018). The B, Na, and Si dissolution rates were comparable to others (Inagaki et al., 2013; Neeway et al., 2018). The localized preferential attack and cracks in the high pH conditions were seen in the ISG samples. The leaching behavior of the ISG samples was also tested as per MCC-1 protocol at 50°C. The formation of C–S–H alteration products during the initial incubation phase led to passivate the dissolution of ISG glass.

The aluminoborosilicate glass was synthesized using the conventional method, and it investigated the roles of Mg and Ca in structure and chemical durability using the PCT-B test (Backhouse et al., 2019). The Na and B leaching rates were obtained in the order of 10^{-3} g $m^{-2}.day^{-1}$ after 112 days. A novel matrix of nanoporous alumino-borosilicate was developed for cesium removal from liquid radioactive waste and its stable immobilization (Abbasi et al., 2020). The matrix showed the maximum Cs sorption (removal of a compound from solution by solid-phase constituents) capacity. The leaching test results of heat-treated samples at 1,100°C have shown the effective stabilization of Cs in the alumina–borosilicate matrix. The effect of cerium doping in borosilicate glass was investigated (Zhu et al., 2019). Ce doping led to an increase in the breakage of B–O–B bonds in [BO_3] units. According to the product consistency test (PCT) results, normalized leaching rates of the main elements (B and Si) and actinide surrogate Ce in the glass were very low.

The stability of aluminoborate glass was studied in the acid, basic, and neutral solutions. The hygroscopic nature of B_2O_3 deteriorates the chemical durability of glass. To avoid this condition, Mascaraque et al. (2019) designed a glass in which the modifier ion content was not more than 25 mol% and the aluminum to boron ratio varied. The increased aluminum content in the glass results in improved chemical durability in the neutral and acidic media, but it is constant in the basic media. It can be concluded that B_2O_3 is highly susceptible to nucleophilic OH^- attack.

Furthermore, durability studies have been found on pharmaceutical glass that contains a mixture of modifier ions in the glass structure. A borosilicate glass was designed with the substitution of CaO with MgO, and the effect of the increased MgO concentration in the glass was observed; furthermore, aqueous stability was tested at 80°C for 40 days (Yang et al., 2021). The borosilicate glass undergoes the whole dissolution mechanism that initiates from the ion exchange process forward to forming a silica-rich layer at the surface of the glass. The increased concentration of MgO led to the deterioration of the chemical durability of glass. The selective leaching of phase-separated iron-containing sodium borosilicate glass was studied (Konon et al., 2022). The chemical durability was affected by Fe^{+3} cations. The acidic treatment on glass led to formation of porous glass (PG), and increasing the time led to an increased pore volume in glass.

The effect of the glass composition and SA/V ratio on the initial and residual rates of leaching was investigated (Gin et al., 2013a). The tests were performed at 90°C after 5 years and compared with SON68 (French inactive R7/T7-type glass). It was found that, with the increase in the SA/V ratio, the normalized leaching rates of Si were decreased. The leaching studies were performed on the SON68 glass under a dynamic test with a higher SA/V ratio (~14,000 m^{-1}) at 90°C. The normalized leaching rate was found in the order of 10^{-4} g $m^{-2}day^{-1}$ at pH 10.5 after 200 days (Neeway et al., 2011). In another study, the leaching behavior of glass was investigated by using ISG as a reference and the leaching mechanism was found (Gin et al., 2013b).

6.2 Chemical durability of ceramic wasteforms

The waste is immobilized into ceramics such as perovskite ($CaTiO_3$), hollandite ($BaAl_2Ti_6O_{16}$), and zirconolite ($CaZrTi_2O_7$) (Barinova et al., 2008). The perovskite/zirconolite matrix can accommodate a wide range of the elements present in HLW. The hollandite–perovskite composite ceramic matrix was synthesized using the solid-state reaction method (Ma et al., 2021). The hollandite and perovskite phases were chosen to immobilize Cs and Sr radionuclides. The chemical durability of the ceramic matrix was tested with the MCC-1 protocol. The normalized leach rate of Sr and Cs was found in the order of 10^{-5} and 10^{-3} g $m^{-2}day^{-1}$ after 42 days, respectively, with the matrix of composition (75% of hollandite and 25% of perovskite). The iodine and cesium radionuclide loading was proposed to be immobilized in the defect perovskite structure named $Cs_3Bi_2I_9$ (Yang et al., 2020). The chemical durability was tested in the form of a silica–ceramic composite matrix (30% silica and 70% perovskite) and a core-shell matrix (80% silica as shell and 20% perovskite as core) with a semi-dynamic leaching experiment for 14 days. The BiOI passivating layer was formed in the silica–ceramic composite matrix, whereas the silica shell prevents the migration of elements in the aqueous media in the case of the silica–perovskite (core-shell structure) matrix. The normalized leach rate of iodine was found to be 30 mg $m^{-2}day^{-1}$ for the silica–ceramic composite matrix and 5.0×10^{-3} g $m^{-2}day^{-1}$ for the core-shell matrix at 90°C.

The powellite ceramic is a potential candidate for immobilizing Mo and minor actinides. A series of ceramics ($Ca_{1-x}Li_{x/2}Gd_{x/2}MoO_4$) was synthesized using a solid-state reaction method, and the sintering temperature was maintained between 525°C and 950°C (Fillet et al., 2004; Frugi et al., 2008; Roessler et al., 2015; Claparede et al., 2017; Meng et al., 2020). The Gd^{+3} ion was taken as a surrogate of minor actinide Cm^{+3}. The normalized mass losses of gadolinium and molybdenum were 1.4×10^{-4} and 2.2×10^{-4} g m^{-2} after 28 days, respectively.

The rare earth phosphates, such as $Gd_{1-x}Yb_xPO_4$ (where x = 0, 0.1, 0.2. . ..1), were synthesized using a solid-state reaction method and sintered at different temperatures ranging from 600°C to 1,600°C (Li et al., 2018). Phase transformation was observed as ytterbium ions replaced gadolinium ions at the lattice site of the ceramic phase. The phase transformation led to distortion in the PO_4 tetrahedra, resulting in decreased elemental leaching. The normalized mass loss of gadolinium and ytterbium was obtained as 2.0×10^{-7} and 2.3×10^{-7} g m^{-2}, respectively, with $Gd_{0.9}Yb_{0.1}PO_4$ composition after 28 days. $Gd_2Zr_2O_7$ was synthesized using the SPS method at a sintering temperature of 1,800°C. The phase was loaded with 45 mol% simulated waste (Wei et al., 2022). The phase transformation occurred from fluorite to pyrochlore after the inclusion of waste. The normalized leach rate of Gd was obtained as 3.5×10^{-8} g $m^{-2}.day^{-1}$ after 42 days with 45 mol% loading of waste. The zirconolite ceramic matrix was synthesized using the solid-state method. Nd (up to 15 at% stabilized) was added as the surrogate of actinides in the matrix (Cai et al., 2016). The leaching study was performed at different pH values (5, 7, and 9) at 90°C. The normalized leach rate of Ca was high at pH = 5 and was obtained as 5.6×10^{-3} g $m^{-2}day^{-1}$ after 42 days. The normalized leaching rate of Nd was almost the same (in the order of ~10^{-5} g $m^{-2}day^{-1}$) at all the pH values. Therefore, the zirconolite matrix was found suitable for immobilizing the Nd radionuclide at different pH values. In addition, the yttrium iron garnet [$Y_{3-x}Ce_xFe_5O_{12}$ ($0 \leq x \leq 1$)] was found to be a potential host for the immobilization of HLW (Luo et al., 2021). The normalized leaching rates of Ce and Y were obtained in the order of 10^{-4} and 10^{-5} g $m^{-2}day^{-1}$ after 42 days, respectively.

6.3 Chemical durability of glass–ceramic wasteforms

The glass–ceramic matrix has gained attention widely due to its ability to immobilize a wide range of actinides. The addition of cerium (Ce) and neodymium (Nd) in the borosilicate glass–ceramic wasteforms (crystalline phase: zirconolite) was investigated, and an aqueous chemical durability test was performed (Zhu et al., 2020a). Nd is invariably used as a nonradioactive or nonactive surrogate of plutonium (Pu) and minor actinides. The aqueous chemical durability was performed through PCT-B and MCC-1 methods at 90°C for 28 days. The normalized leach rates of elements (Si, Ca and Nd) were obtained as 4.5×10^{-3}, 2.5×10^{-3}, and 1.2×10^{-4} g $m^{-2}day^{-1}$ with the MCC-1 method, respectively (with 20 wt % of CeO_2 + 20 wt% Nd_2O_3), and the concentration of Ce in leachate was found negligible. It was also reported that with an increase in the loading % from 15 to 40 of Nd and Ce (in equal amount), an oxyapatite phase appeared in the glass–ceramics, and the appeared phase did not significantly influence the chemical durability of glass–ceramics.

A glass–ceramic wasteform containing calcium neodymium cerium oxide silicate [$Ca_2Nd_{8-x}Ce_x(SiO_4)_6O_2$] as the ceramic phase was synthesized to immobilize the rare-earth ions in wastes generated by pyro-processing (Kim and Heo, 2015). The normalized leach rate values of Nd and Ce were obtained as 2.2×10^{-6} and 2.6×10^{-6} g $m^{-2}.day^{-1}$, respectively, from the PCT test, and the leach rate values were found to be <0.1 ppb from the MCC-1 test performed at 90°C for 35 days. The normalized leach rates of elements were lower in glass–ceramic compared to the glass matrix. The zirconolite–sodium borosilicate glass–ceramic wasteforms were prepared using the one-step slow cooling method (Zhu et al., 2020b). The normalized leach rates of Si, Ca, and Ce were found to be minimal even after 56 days. The zirconolite–borosilicate glass–ceramic matrix had shown good aqueous durability and was found suitable for immobilizing HLW. The barium borosilicate glass–ceramic containing CTZ (Molar ratio of CaO, TiO_2, and $ZrSiO_4$—2:2:1) was prepared with the addition of 0, 45, and 55 wt% CTZ in the glass (Li et al., 2015). The CTZ45 glass–ceramic matrix (annealed at 950°C) showed lower normalized leaching rates. The normalized leaching rates of Na, B, and Nd were obtained as 7.7×10^{-3}, 8.8×10^{-3}, and 7.5×10^{-6} g $m^{-2}day^{-1}$, respectively after 28 days. However, glass (CTZ0 matrix) was not chemically durable. The CTZ55 glass–ceramic matrix had multiple crystalline phases, resulting in decreased network formers and poor chemical durability. Therefore, the CTZ45 glass–ceramic matrix was found to be the most chemically durable.

The barium borosilicate glass–ceramics were synthesized with neodymium oxide (0–12 wt%) (Wu et al., 2016). The loading of

Nd_2O_3 in the range of 2–6 wt% results in mainly zirconolite and titanate phases, whereas increasing the content of Nd_2O_3 up to 8 wt % led to the formation of the titanate phase only. The normalized leach rate of the glass–ceramics with 6 wt% loading of Nd_2O_3 was low compared to 8 wt% loading in the glass–ceramic matrix. The normalized leach rates of Nd, Ca, and B were 4.4×10^{-6}, 1.6×10^{-3}, and 6.8×10^{-3} g m^{-2}.day^{-1}, respectively, with a loading of 6 wt% Nd_2O_3 glass–ceramics after 42 days. Furthermore, the zirconolite barium borosilicate glass–ceramics with simulated sulfate containing liquid waste (0, 16, 20, 30 wt%) was synthesized (Wu et al., 2018). The zirconolite phase and some minor baddeleyite phases were present at 16 wt% liquid waste loading. In contrast, increasing the content of liquid waste (20–30 wt%) led to the perovskite phase formation. The normalized leaching rates of Si, B, Na, and La were obtained as 8.1×10^{-4}, 1.6×10^{-3}, 7.2×10^{-3}, and 1.2×10^{-3} g $m^{-2}day^{-1}$, respectively, after 28 days with 16 wt% liquid waste content. The zirconolite barium borosilicate glass–ceramic matrices were prepared with the loading of the SO_3 content (0, 2, 6, and 8 wt%) (Wang et al., 2017). The matrix with 4 wt% of SO_3 content led to a new barite phase. The normalized leach rates of Si, B, and Ba were found in the order of 10^{-3}, 10^{-3}, and 10^{-4} g m^{-2}.day^{-1} after 14 days, respectively. The 8 wt% SO_3-loaded glass–ceramic matrix had shown higher leaching rates because it had pores and an unstable nardite phase, leading to poor chemical durability.

The pyrochlore-based borosilicate glass–ceramics were synthesized at 1,300°C and cooled to 1,050°C at the rate of 10°C min^{-1} using the one-step heat treatment method with a uniform distribution of the crystalline phase (Wu et al., 2020). The normalized leach rates of Na, B, Al, Si, Nd, Ti, and Nb were obtained as 6.8×10^{-3}, 3.7×10^{-4}, 1.5×10^{-2}, 2.2×10^{-3}, 3.0×10^{-5}, 5.1×10^{-5}, and 5.5×10^{-6} g $m^{-2}day^{-1}$ after 28 days, respectively. The borosilicate glass–ceramics were synthesized with the loading of the strontium oxide content in the range of 10–25 mol% (Pilania et al., 2023). The normalized leach rates of Si, B, and Sr were obtained as 1.2×10^{-8}, 3.7×10^{-9}, and 1×10^{-8} g $m^{-2}day^{-1}$ after 30 days, respectively.

7 Radiation stability of wasteforms

In addition to chemical durability, the radiation stability of the wasteforms/matrices plays a major role in selecting a matrix. The actinides in the radioactive waste emit alpha particles and recoil nuclei (Weber et al., 1998). The recoil nucleus undergoes several cascade collisions within the matrix. These primary and secondary collisions lead to defect generation within the matrix. The radiation stability of different types of matrices is reviewed in the following section.

7.1 Radiation stability of glass wasteforms

In order to obtain radiation-resistant wasteforms, efforts are being made to explore a matrix with moderate radiation resistance. The radiation stability of borosilicate glass was investigated by electron paramagnetic resonance and ultraviolet-visible spectroscopy (Wang et al., 2020). The glass samples were exposed to ^{60}Co gamma radiation with a dose rate of 5,560 Gy h^{-1}, and we observed an increase in non-bridging oxygen (NBO) ions, formation of peroxy radical, etc., which were detrimental for the structural integrity of the matrix. The gamma irradiation effect on the Fe- and Eu-doped Trombay nuclear waste glass was investigated through electron spin resonance and photoluminescence spectroscopy (Mohapatra et al., 2014). The ^{60}Co gamma source was irradiated at doses 1 kGy h^{-1} and 8 kGy h^{-1}. Europium (Eu^{+3}) was used as a surrogate for plutonium (Pu^{+3}) in the glass matrix. The PL results showed the stability of trivalent species in the matrix. The formation of the Eu^{+2} oxidation state was not observed in the glass, but Eu sites were more disordered after gamma irradiation (de Bonfils et al., 2007). The effects of beta irradiation on the 30 mol% Fe_2O_3-70 mol% P_2O_5 polyphosphate glass were studied. The glass was irradiated with a beta emitter ^{90}Sr/^{90}Y source (varying dose from 5.4 to 22 kGy) (Goj et al., 2019). The glass structure led to the breakage of P–O–P bonding upon irradiation, and the broken bonds might form the P–O–H bridges, which can decrease the chemical durability. The knocking out process of phosphorous can create the P–O–O–P linkage, which also relaxes in the form of P–O–P bridges and O_2 (oxygen bubbles). The Fe–O–P bridges were radiation-tolerant, as compared to P–O–P bridges. In another study on iron phosphate glass (IPG: $45Fe_2O_3$-$55P_2O_5$ in mol%) using electron beam irradiation, an increase in electron dose from 1×10^{26} to 4.8×10^{26} e m^{-2} led to the formation of Fe-rich and P-rich nanophases along with phase separation (Sun et al., 2003). Self-heating and charging were anticipated factors that led to the structural changes in IPG. In order to investigate the effect of the ^{137}Cs radionuclide on the radiation stability of sodium alumino-iron phosphate glass, Ba was taken as a surrogate of Cs (Stefanovsky et al., 2019). The Ba replacement for Cs exhibited a slight modification in the glass network but no substantial effects on the hydrolytic durability of the phosphate glass. There was no change observed in the Fe^{3+} to Fe^{2+} ratio.

The samples become radioactive after irradiation in existing gamma and beta sources; therefore, induced activity inhibits detailed investigation of irradiated samples. In addition, the availability of irradiation sources and energy is limited. To overcome the activity of irradiated samples, the ion irradiation method can be used as a surrogate method with the added advantage of desired fluence and energy. The ion-irradiated samples do not get activated and can be tested in the existing laboratory setup. Similar conditions can be simulated with high-energy ion beams, and radiation stability can be performed (Dube et al., 2015). The radiation stability of iron phosphate glass was studied by (Dube et al., 2020), in which cerium was used as a surrogate of actinides. The pure and cerium-doped iron phosphate glass (IPG) was irradiated with a gold source of energy 750 keV at a fluence of 2×10^{15} ion cm^{-2} to mimic ballistic damage due to the cascade of recoil atoms during the decay of actinides. The Raman spectra confirmed the incorporation of cerium as a modifier in the glass. A significant reduction of iron was observed after gold ion irradiation. The iron reduction might lead to the formation of crystals, so poor chemical durability of cerium-doped glass was anticipated. Swift heavy ion irradiation using 14.4 MeV Si ions at a fluence of 1×10^7 ions cm^{-2} on zinc phosphate glass showed the formation of ion tracks and reduced the number of bridging O atoms (Awazu et al., 2003). The heavy ion irradiation using 4 MeV O^+ ions from 5×10^{13} to 5×10^{16} ion cm^{-2}

on IPG leads to the formation of nanocrystals with different phases, such as $Fe_4(P_2O_7)_3$ and $Fe(PO_3)_3$. The ion track was formed upon irradiation, owing to stress in the matrix, which results in considerable deformation (shear bands). The shear bands led to the formation of nanocrystals (Jegadeesan et al., 2015).

7.2 Radiation stability studies on ceramic wasteforms

The ceramic wasteforms exhibit long-term stability, radiation tolerance, and leaching resistance, and most of the actinides and fission products can be incorporated into polycrystalline phases (Weber et al., 1998). A synroc is a widely known ceramic for the immobilization of minor actinides, which are generated from the nuclear fuel cycle and reprocessing of fuel. The synroc consists of hollandite, perovskite, and zirconolite phases. Among these phases, zirconolite has a better radiation stability, aqueous corrosion resistance, and thermal stability (Rossell, 1992). Several attempts have been made to study the radiation-induced modification in the zirconolite matrix. The radiation stability of zirconolite ceramics was investigated using a surrogate method of ion irradiation. The matrix was bombarded with He^+ ions (30 keV) at fluence ranging from 1×10^{17} to 1×10^{21} ions cm^{-2} (Gupta et al., 2016). The XRD results of irradiated samples revealed the damage at fluence 1×10^{20} ions cm^{-2}, and the decrease in intensity of the XRD peaks with the increase in fluence was attributed to the radiation-induced defects in the matrix. However, the monoclinic structure was intact even at the maximum fluence used for the study. Nd-doped zirconolite and perovskite (Nd as Pu surrogate) were irradiated with Kr^+ ions of energy 2 MeV at a fluence of 5×10^{15} ions cm^{-2} (Davoisne et al., 2011). The micro-diffraction patterns revealed radiation-induced structural changes in the Nd-doped perovskite matrix, which indicated the symmetry change (from orthorhombic to cubic) along with matrix amorphization.

Nd-doped zirconolite pellets were irradiated with He^+ ions (30 keV) to observe the irradiation-induced effects in the matrix (Gupta et al., 2020). A decrease in intensity and an increase in the width of the peaks at the fluence of 1×10^{17} ions cm^{-2} in XRD peaks were observed without loss of significant crystallinity. It was anticipated that an increase in the fluence of He^+ ions can lead to the formation of helium bubbles in the matrix. Consequently, the radiation stability property of the matrix might get deteriorated. The same group further studied the effects of Au (120 MeV) ion irradiation on the Nd-doped zirconolite to simulate the α-decay events at a fluence of 3×10^{13} ions cm^{-2} (Gupta et al., 2019). The broadening and reduction in the intensity of the XRD peaks confirmed the induced defects and vacancies at the fluence of 3×10^{13} ions cm^{-2}. The heavy ion irradiation-induced amorphous track formation was observed in the matrix. The irradiation effect on the pyrochlore ceramic matrix ($A_2Ti_2O_7$; where A: Y, Sm, Gd, Er, and Yb) was investigated with ^{197}Au ions (2.2 GeV) (Shamblin et al., 2016). The amorphous nature and track formation were observed in all compositions. The $Y_2Ti_2O_7$ ceramic was more amorphous resistant than other compositions, whereas $Gd_2Ti_2O_7$ was prone to amorphization.

The Nd-doped zirconolite ($(Ca_{0.8}Nd_{0.2})Zr(Ti_{1.8}Al_{0.2})O_7$) ceramic was irradiated with i) Kr^+ ions (2 MeV) at a fluence of 1×10^{14} and 5×10^{15} ions cm^{-2} and ii) He^+ ions (200 keV) at a fluence of 1×10^{14}, 5×10^{15}z and 1×10^{17} ions cm^{-2} (Gilbert et al., 2011). There was no significant damage at a lower fluence of both the ions; however, at a higher fluence (5×10^{15} ions cm^{-2}) of Kr^+ ions, zirconolite got completely amorphized, whereas helium accumulation or helium bubbles were observed at a high fluence of He^+ ions. The radiation-induced modifications in the single-crystal yttria-stabilized zirconolite (YSZ) ceramic using He^+ ions (100 keV) have been studied (Yang et al., 2012). An effort was made to investigate the damage evolution process in three fluence regimes: i) at a low fluence in the range of 1×10^{16} to 4×10^{16} ions cm^{-2}, formation of point defects was seen; ii) at an intermediate fluence in the range of 8×10^{16} to 1×10^{17} ions cm^{-2}, volume defect clusters were seen; iii) at a fluence of 2×10^{17} and 4×10^{17} ions cm^{-2}, ribbon-like He bubbles and cracks were observed, which cause the blistering on the surface. A similar study was performed on polycrystalline yttria-stabilized zirconolite ceramics, which were irradiated with He^+ ions (70 keV). The single crystal and polycrystalline samples of YSZ had shown similar behavior (spherical and ribbon-like helium bubbles of different shapes under irradiation) (Yang et al., 2015a).

The decay of ^{90}Sr emits beta particles of energy in the range of 0.546–2.28 MeV. The interaction of beta particles and generated recoil nuclei in ceramic wasteforms led to the deterioration in the physical properties of the matrix (Aubin-Chevaldonnet et al., 2006). Therefore, ceramic wasteforms are desired to be stable under the beta decay of Sr. In order to simulate the effect of energetic beta particles on the radiation stability of ceramic wasteforms, strontium titanate was irradiated with an electron beam of energy 1.8 MeV with a flux of 1.5×10^{13} electrons/$cm^2.s^1$ (Yang et al., 2015b). The energetic electrons can produce atomic displacements by depositing energy to the matrix, which may induce phase separation, chemical disordering, or amorphization in irradiated materials (Kinsho et al., 2003). The perovskite structure did not change after electron irradiation, as revealed from the Raman spectrum of $SrTiO_3$. The electron microscopic images revealed a dense microstructure, which was advantageous to avoid radioactive nuclide leaking into the environment. The $CaZrO_3$ perovskite was irradiated with the Au^+ ions (940 MeV) at a fluence of 1.5×10^{13} ions cm^{-2} (Lang et al., 2012). Perovskite got completely amorphized, and amorphous tracks of size 6 ± 0.6 nm were seen.

The polycrystalline pyrochlore ($Lu_2Ti_2O_7$) was irradiated with the beam of He^+ ions (200 keV) in a fluence ranging 2×10^{15}—2×10^{17} ions cm^{-2} (Zhang et al., 2015). Micro-swelling was observed at the fluence of more than 2×10^{16} ions cm^{-2}; on further increase in the fluence, the matrix turned into a completely disordered structure. The pristine pyrochlore phase was intact up to a fluence of 5×10^{16} ions cm^{-2}, and at higher fluence, order to disorder transformation was seen. The amorphization of pyrochlore was not observed even at a fluence of 2×10^{17} ions cm^{-2}. The radiation stability of $Gd_2Zr_2O_7$ pyrochlore with Au^{+3} ions (7 MeV) at a fluence of 2.2×10^{15} ions cm^{-2} was investigated (Taylor et al., 2016). The samples irradiated with Au^{+3} ions underwent pyrochlore-to-defect fluorite structure transformation, and swelling was also seen. Subsequently, the irradiated samples were bombarded with He^+ ions at a fluence of 2×10^{15} and 2×10^{16} ions cm^{-2}; furthermore, an increase in lattice swelling was seen. The lattice swelling was decreased at a higher fluence of 2×10^{17} ions cm^{-2} (Debelle et al., 2010).

7.3 Radiation stability studies on glass–ceramic wasteforms

In order to determine the radiation stability of glass–ceramic matrices, the borosilicate glass–ceramic matrices incorporating Cs/Sr (CS), lanthanide (LN), and transition metal (TM)) were investigated under different irradiation conditions (Tang et al., 2014). The samples were irradiated with a high-energy (5 MeV) alpha ion beam at a fluence of 1×10^{21} ions m^{-2} and a low-energy (600 keV) Kr heavy-ion beam at a fluence of 2.5×10^{19} ions m^{-2} to observe self-irradiation effects in the matrix. The light-ion beam (alpha ion) did not induce structural changes in the matrix, whereas the heavy-ion beam (Kr ion) led to a change from crystalline phases into an amorphous phase. The electron irradiation study was performed at a dose of 10^{13} Gy (equivalent to 1,000 years of Cs/Sr-loaded wasteform irradiation dose (Weber et al., 2009)) to observe the changes in the ceramic phase. The studies show that the matrix was radiation-tolerant under β- and γ-beam irradiation. The radiation stability of the zirconolite-based aluminosilicate glass–ceramic matrix was investigated (Mir et al., 2021). The matrix was irradiated with a He ion beam at different energies and fluence. The 10-keV He ions at a fluence of 8×10^{16} He cm^{-2} h led to the formation of He bubbles in the ceramic phase and oxygen bubbles in the glass phase. Helium bubble formation was not observed in the glass phase, which may be due to a large He diffusion coefficient. The amorphization of the zirconolite phase was observed with 20-keV He ion irradiation at a fluence of 1.2×10^{17} He cm^{-2} at 143 k temperature.

8 Summary

The review uncovers broader aspects of matrices for radioactive waste immobilization. An introduction to wasteforms and types of wasteforms for radioactive waste immobilization are discussed. The glass, ceramic, and glass–ceramic wasteforms are introduced and reviewed in detail. The glass–ceramic wasteforms revolutionized have given a new perspective for the immobilization of radionuclides. However, glass–ceramics are still under exploration. Glass–ceramics can be potential wasteforms for the immobilization of waste generated from next-generation nuclear reactors.

The immobilization of spent metallic fuels generated from next-generation nuclear reactors needs to be addressed. The reprocessing of used fuel to recover uranium reduces the wastage of uranium and plutonium. Long-lived actinides are being reprocessed to be converted into short-lived actinides. Short-lived actinides along with traces of long-lived actinides can be immobilized in suitable glass–ceramic wasteforms. In addition, spreading awareness about storage among the public should be considered. At proposed storage/disposal sites, a series of awareness campaigns should be conducted to educate the public.

Author contributions

RP contributed to the literature review and writing of the manuscript. CD presented the idea to conceptualize the article, and gave critical comments and suggestions to improve the manuscript.

Acknowledgments

The authors received the financial assistance from UGC and infrastructure from CUG, Gandhinagar, for the work.

Conflict of interest

The authors declare that the research was conducted in the absence of any commercial or financial relationships that could be construed as a potential conflict of interest.

Publisher's note

References

Abbasi, A., Davarkhah, R., Avanes, A., Yadollahi, A., Ghannadi-Maragheh, M., and Sepehrian, H. (2020). Development of nanoporous alumino-borosilicate as a novel matrix for the sorption and stable immobilization of cesium ions. *J. Inorg. Organomet. Polym. Mater.* 30, 369–378. doi:10.1007/s10904-019-01195-z

Abrajano, T. A., Bates, J. K., and Byers, C. D. (1986). Aqueous corrosion of natural and nuclear waste glasses I. Comparative rates of hydration in liquid and vapor environments at elevated temperatures. *J. Non Cryst. Solids.* 84 (1-3), 251–257. doi:10.1016/0022-3093(86)90783-0

Aldean, I., Sun, S. K., Wilkins, M. C. D., Gardner, L. J., Mason, A. R., Stennett, M. C., et al. (2022). Synthesis and characterisation of Ce-doped zirconolite $Ca_{0.80}Ce_{0.20}ZrTi_{1.60}M_{0.40}O_7$ (M = Fe, Al) formed by reactive spark plasma sintering (RSPS). *MRS Adv.* 7, 75–80. doi:10.1557/S43580-022-00221-6

Aubin-Chevaldonnet, V., Gourier, D., Caurant, D., Esnouf, S., Charpentier, T., and Costantini, J. M. (2006). Paramagnetic defects induced by electron irradiation in barium hollandite ceramics for caesium storage. *J. Phys. Condens. Matter.* 18, 4007–4027. doi:10.1088/0953-8984/18/16/009

Awazu, K., Roorda, S., Brebner, J. L., Ishii, S., and Shima, K. (2003). Structure of latent tracks created by swift heavy ions in amorphous SiO_2 and zinc phosphate glass. *Jpn. J. Appl. Phys.* 42, 3950–3957. doi:10.1143/JJAP.42.3950

Backhouse, D. J., Corkhill, C. L., Hyatt, N. C., and Hand, R. J. (2019). Investigation of the role of Mg and Ca in the structure and durability of aluminoborosilicate glass. *J. Non Cryst. Solids.* 512, 41–52. doi:10.1016/j.jnoncrysol.2019.03.003

Backhouse, D. J., Fisher, A. J., Neway, J. J., Corkhill, C. L., Hyatt, N. C., and Hand, R. J. (2018). Corrosion of the international simple glass under acidic to hyperalkaline conditions. *npj Mater. Degrad.* 2, 29. doi:10.1038/s41529-018-0050-5

Barinova, T. V., Borovinskaya, I. P., Ratnikov, V. I., and Ignat'eva, T. I. (2008). Self-propagating high-temperature synthesis for immobilization of high-level waste in mineral-like ceramics: 1. Synthesis and study of titanate ceramics based on perovskite and zirconolite. *Radiochemistry* 50, 316–320. doi:10.1134/S1066362208030181

Baumgärtner, F., and Ertel, D. (1980). The modern purex process and its analytical requirements. *J. Radioanal.* 58, 11–28. doi:10.1007/BF02533770

Beckitt, S. (2012). *Decommissioning of legacy nuclear waste sites: Dounreay, UK, nuclear decommissioning planning, execution and international experience*. Cambridge: Woodhead Publishing, 701–744. doi:10.1533/9780857095336.3.701

Bunker, B. C., Arnold, G. W., and Wilder, J. A. (1984). Phosphate glass dissolution in aqueous solutions. *J. Non Cryst. Solids.* 64 (3), 291–316. doi:10.1016/0022-3093(84)90184-4

Cai, X., Teng, Y., Wu, L., Zhang, K., and Huang, Y. (2016). The synthesis and chemical durability of Nd-doped single-phase zirconolite solid solutions. *J. Nucl. Mater.* 479, 455–460. doi:10.1016/j.jnucmat.2016.07.042

Claparede, L., Guigue, M., Jouan, G., Nadah, N., Dacheux, N., and Moisy, P. (2017). Long-term behavior of refractory thorium-plutonium dioxide solid solutions. *J. Nucl. Mater.* 483, 158–166. doi:10.1016/J.JNUCMAT.2016.11.007

Clark, B. M., Tumurugoti, P., Sundaram, S. K., Amoroso, J. W., and Marra, J. C. (2021). Preparation and characterization of multiphase ceramic designer waste forms. *Sci. Rep.* 11, 4512. doi:10.1038/s41598-021-84014-1

Clark, D. E., and Zoitos, B. K. (1992). *Corrosion of glass, ceramics and ceramic superconductors: Principles, testing, characterization and applications*. United States: Noyes Publications.

Corkhill, C. L., Cassingham, N. J., Heath, Paul.G., and Hyatt, N. C. (2013). Dissolution of UK high-level waste glass under simulated hyperalkaline conditions of a colocated geological disposal facility. *Int. J. Appl. Glass Sci.* 4, 341–356. doi:10.1111/ijag.12042

Crovisier, J.-L., Advocat, T., and Dussossoy, J.-L. (2003). Nature and role of natural alteration gels formed on the surface of ancient volcanic glasses (Natural analogs of waste containment glasses). *J. Nucl. Mater.* 321 (1), 91–109. doi:10.1016/S0022-3115(03)00206-X

Darda, S. A., Gabbar, H. A., Damideh, V., Aboughaly, M., and Hassen, I. (2021). A comprehensive review on radioactive waste cycle from generation to disposal. *J. Radioanal. Nucl. Chem.* 329, 15–31. doi:10.1007/S10967-021-07764-2

Davis, M. J., and Zanotto, E. D. (2017). Glass-ceramics and realization of the unobtainable: property combinations that push the envelope. *MRS Bull.* 42, 195–199. doi:10.1557/MRS.2017.27

Davoisne, C., Stennett, M. C., Hyatt, N. C., Peng, N., Jeynes, C., and Lee, W. E. (2011). Krypton irradiation damage in Nd-doped zirconolite and perovskite. *J. Nucl. Mater.* 415, 67–73. doi:10.1016/j.jnucmat.2011.05.043

de Bonfils, J., Panczer, G., de Ligny, D., Peuget, S., and Champagnon, B. (2007). Behaviour of simplified nuclear waste glasses under gold ions implantation: A microluminescence study. *J. Nucl. Mater.* 362, 480–484. doi:10.1016/j.jnucmat.2007.01.101

Debelle, A., and Declémy, A. (2010). XRD investigation of the strain/stress state of ion-irradiated crystals. *Nucl. Instrum. Methods Phys. Res. B* 268, 1460–1465. doi:10.1016/j.nimb.2010.01.009

Donald, I. W., Metcalfe, B. L., and Taylor, R. N. J. (1997). The immobilization of high-level radioactive wastes using ceramics and glasses. *J. Mater. Sci.* 32, 5851–5887. doi:10.1023/A:1018646507438

Donald, I. W. (2010). *Waste immobilization in glass and ceramic based hosts: Radioactive, toxic and hazardous wastes*. doi:10.1002/9781444319354

Dube, C. L., Kulriya, P. K., Dutta, D., Pujari, P. K., Patil, Y., Mehta, M., et al. (2015). Positron annihilation lifetime measurement and X-ray analysis on 120 MeV Au^{+7} irradiated polycrystalline tungsten. *J. Nucl. Mater.* 467, 406–412. doi:10.1016/j.jnucmat.2015.05.029

Dube, C. L., Stennett, M. C., Ananthanarayanan, A., David, C., Shah, J. G., and Hyatt, N. C. (2020). Radiation stability study on cerium loaded iron phosphate glasses by ion irradiation method. *J. Radioanal. Nucl. Chem.* 323, 1381–1386. doi:10.1007/s10967-020-07012-z

Englert, M., Krall, L., and Ewing, R. C. (2012). Is nuclear fission a sustainable source of energy? *MRS Bull.* 37, 417–424. doi:10.1557/MRS.2012.6

Ewing, R. C., Weber, W. J., and Lian, J. (2004). Nuclear waste disposal—pyrochlore ($A_2B_2O_7$): nuclear waste form for the immobilization of plutonium and "minor" actinides. *J. Appl. Phys.* 95 (11), 5949–5971. doi:10.1063/1.1707213

Fillet, C., Advocat, T., Bart, F., Leturcq, G., and Rabiller, H. (2004). Titanate-based ceramics for separated long-lived radionuclides. *Comptes. Rendus. Chim.* 7, 1165–1172. doi:10.1016/J.CRCI.2004.02.018

Frugier, P., Gin, S., Minet, Y., Chave, T., Bonin, B., Godon, N., et al. (2008). SON68 nuclear glass dissolution kinetics: current state of knowledge and basis of the new GRAAL model. *J. Nucl. Mater.* 380, 8–21. doi:10.1016/J.JNUCMAT.2008.06.044

Gilbert, M., Davoisne, C., Stennett, M., Hyatt, N., Peng, N., Jeynes, C., et al. (2011). Krypton and helium irradiation damage in neodymium–zirconolite. *J. Nucl. Mater.* 416, 221–224. doi:10.1016/j.jnucmat.2010.11.089

Gin, S., Abdelouas, A., Criscenti, L. J., Ebert, W. L., Ferrand, K., Geisler, T., et al. (2013b). An international initiative on long-term behavior of high-level nuclear waste glass. *Mater. Today* 16, 243–248. doi:10.1016/J.MATTOD.2013.06.008

Gin, S., Frugier, P., Jollivet, P., Bruguier, F., and Curti, E. (2013a). New insight into the residual rate of borosilicate glasses: effect of S/V and glass composition. *Int.J. Appl. Glass Sci.* 4 (4), 371–382. doi:10.1111/IJAG.12048

Gin, S., Guittonneau, C., Godon, N., Neff, D., Rebiscoul, D., Cabí, M., et al. (2011). Nuclear glass durability: new insight into alteration layer properties. *J. Phys. Chem. C* 115, 18696–18706. doi:10.1021/JP205477Q

Gin, S., Mir, A. H., Jan, A., Delaye, J. M., Chauvet, E., De Puydt, Y., et al. (2020). A general mechanism for gel layer formation on borosilicate glass under aqueous corrosion. *J. Phys. Chem. C* 124 (9), 5132–5144. doi:10.1021/ACS.JPCC.9B10491

Goj, P., Jeleń, P., Marczewska, B., and Stoch, P. (2019). Effect of β-Irradiation on the structure of iron polyphosphate glass. *J. Nucl. Mater.* 523, 198–205. doi:10.1016/j.jnucmat.2019.06.014

Gupta, M., Kulriya, P. K., Kumar, R., and Ghumman, S. S. (2020). Structural investigation of Nd-zirconolite irradiated with He+ ions. *J. Radioanal. Nucl. Chem.* 323, 1413–1418. doi:10.1007/s10967-019-06873-3

Gupta, M., Kulriya, P. K., Meena, R. C., Neumeier, S., and Ghumman, S. S. (2019). Probing swift heavy ion irradiation damage in Nd-doped zirconolite. *Nucl. Instrum. Methods Phys. Res. B* 453, 22–27. doi:10.1016/j.nimb.2019.06.002

Gupta, M., Kulriya, P. K., Shukla, R., Dhaka, R. S., Kumar, R., and Ghumman, S. S. (2016). Reduction and structural modification of zirconolite on He+ ion irradiation. *Nucl. Instrum. Methods Phys. Res. B* 379, 119–125. doi:10.1016/j.nimb.2016.04.020

Herbst, R. S., Baron, P., and Nilsson, M. (2011). *Standard and advanced separation: PUREX processes for nuclear fuel reprocessing, advanced separation techniques for nuclear fuel reprocessing and radioactive waste treatment*. Cambridge: Woodhead Publishing, 141–175. doi:10.1533/9780857092274.2.141

Hopf, J., Eskelsen, J. R., Chiu, M., Ievlev, A. V., Ovchinnikova, O. S., Leonard, D., et al. (2018). Toward an understanding of surface layer formation, growth, and transformation at the glass–fluid interface. *Geochim. Cosmochim. Acta.* 229, 65–84. doi:10.1016/j.gca.2018.01.035

Hyatt, N. C., and Ojovan, M. I. (2019). Special issue: materials for nuclear waste immobilization. *Materials* 12 (21), 3611. doi:10.3390/ma12213611

IAEA Safety Standards (2009). Classification of radioactive waste for protecting people and the environment No. GSG-1 general safety guide. Available at: http://www-ns.iaea.org/standards.

IAEA (2017). *Selection of technical solutions for the management of radioactive waste*. Vienna, Austria: IAEA TECDOC SERIES.

Inagaki, Y., Kikunaga, T., Idemitsu, K., and Arima, T. (2013). Initial dissolution rate of the international simple glass as a function of ph and temperature measured using microchannel flow-through test method. *Int. J. Appl. Glass Sci.* 4, 317–327. doi:10.1111/IJAG.12043

Jantzen, C. M. (2011). "Development of glass matrices for high level radioactive wastes," in *Handbook of advanced radioactive waste conditioning technologies* (Cambridge: Woodhead Publishing), 230–292. doi:10.1533/9780857090959.2.230

Jantzen, C. M., Lee, W. E., and Ojovan, M. I. (2013). "Radioactive waste (RAW) conditioning, immobilization, and encapsulation processes and technologies: overview and advances," in *Radioactive waste management and contaminated site clean-up: Processes, technologies and international experience* (Cambridge: Woodhead Publishing), 171–272. doi:10.1533/9780857097446.1.171

Jantzen, C. M., and Ojovan, M. I. (2019). On selection of matrix (wasteform) material for higher activity nuclear waste immobilization (review). *Russ. J. Inorg. Chem.* 64, 1611–1624. doi:10.1134/S0036023619130047

Jegadeesan, P., Amirthapandian, S., Joseph, K., David, C., Panigrahi, B. K., and Kutty, K. V. G. (2015). Ion irradiation induced crystallization in iron phosphate glass – TEM investigations. *Adv. Mater. Lett.* 6, 224–227. doi:10.5185/amlett.2015.5725

Jo, Y., Garbev, K., Çevirim-Papaioannou, N., Blanco, O. D., de Blochouse, B., Altmaier, M., et al. (2022). Solubility of niobium(V) in cementitious systems relevant for nuclear waste disposal: characterization of the solubility-controlling solid phases. *J. Hazard. Mater.* 440, 129810. doi:10.1016/J.JHAZMAT.2022.129810

Kavaz, E., El_Agawany, F. I., Tekin, H. O., Perişanoğlu, U., and Rammah, Y. S. (2020). Nuclear radiation shielding using barium borosilicate glass ceramics. *J. Phys. Chem. Solids.* 142, 109437. doi:10.1016/j.jpcs.2020.109437

Khan, S., Syed, A. T., Ahmad, R., Rather, T. A., Ajad, M., and Jan, F. A. (2010). Radioactive waste management in a hospital. *Int. J. Health Sci.* 4 (1), 39–46.

Kim, M., and Heo, J. (2015). Calcium-borosilicate glass-ceramics wasteforms to immobilize rare-earth oxide wastes from pyro-processing. *J. Nucl. Mater.* 467, 224–228. doi:10.1016/j.jnucmat.2015.09.040

Kinsho, M., Saito, Y., Nishizawa, D., and Michizono, S. (2003). 2.5 MeV electron irradiation effect of alumina ceramics. *J. Nucl. Mater.* 318, 307–312. doi:10.1016/S0022-3115(03)00018-7

Knox, M., and Copley, G. (1997). Use of microwave radiation for the processing of glass. *Glass Technol.* 38, 91–96.

Konon, M., Antropova, T., Zolotov, N., Simonenko, T., Simonenko, N., Brazovskaya, E., et al. (2022). Chemical durability of the iron-containing sodium borosilicate glasses. *J. Non Cryst. Solids.* 584, 121519. doi:10.1016/j.jnoncrysol.2022.121519

Kumari, I., Kumar, B. V. R., and Khanna, A. (2020). A review on UREX processes for nuclear spent fuel reprocessing. *Nucl. Eng. Des.* 358, 110410. doi:10.1016/J.NUCENGDES.2019.110410

Lang, M., Zhang, F., Li, W., Severin, D., Bender, M., Klaumünzer, S., et al. (2012). Swift heavy ion-induced amorphization of $CaZrO_3$ perovskite. *Nucl. Instrum. Methods Phys. Res. B* 286, 271–276. doi:10.1016/j.nimb.2011.12.028

Lee, W. E., Ojovan, M. I., Stennett, M. C., and Hyatt, N. C. (2006). Immobilisation of radioactive waste in glasses, glass composite materials and ceramics. *Adv. Appl. Ceram.* 105, 3–12. doi:10.1179/174367606X81669

Lee, W. E., Ojovan, M. I., and Jantzen, C. M. (2013b). *Radioactive waste management and contaminated site clean-up processes, technologies and international experience*. Amsterdam, Netherlands: Elsevier.

Lee, W. E., Ojovan, M. I., and Jantzen, C. M. (2013a). *Radioactive waste management and contaminated site clean-up: Processes, technologies and international experience*. Cambridge: Woodhead Publishing.

Li, H., Wu, L., Xu, D., Wang, X., Teng, Y., and Li, Y. (2015). Structure and chemical durability of barium borosilicate glass–ceramics containing zirconolite and titanite crystalline phases. *J. Nucl. Mater.* 466, 484–490. doi:10.1016/J.JNUCMAT.2015.08.031

Li, J., Xu, D., Wang, X., Liu, K., Mao, Y., Wang, M., et al. (2021). Encapsulation of cesium with a solid waste-derived sulfoaluminate matrix: A circular economy approach of treating nuclear wastes with solid wastes. *J. Hazard. Mater.* 416, 126156. doi:10.1016/J.JHAZMAT.2021.126156

Li, W., Ding, X., Meng, C., Ren, C., Wu, H., and Yang, H. (2018). Phase structure evolution and chemical durability studies of $Gd_{1-x}Yb_xPO_4$ ceramics for immobilization of minor actinides. *J. Mater. Sci.* 53, 6366–6377. doi:10.1007/S10853-018-2031-Z

Luo, S., Xu, Z., Liu, J., Xu, B., Ji, S., Ding, Y., et al. (2021). The solubility, microstructure, and chemical durability of Ce-doped YIG ceramics designed as actinide waste forms. *Int. J. Energy Res.* 45, 19883–19894. doi:10.1002/ER.7058

Ma, J., Fang, Z., Yang, X., Wang, B., Luo, F., Zhao, X., et al. (2021). Investigating hollandite–perovskite composite ceramics as a potential waste form for immobilization of radioactive cesium and strontium. *J. Mater. Sci.* 56, 9644–9654. doi:10.1007/S10853-021-05886-2

Ma, L., Brow, R. K., and Schlesinger, M. E. (2017). Dissolution behavior of Na_2O–FeO–Fe_2O_3–P_2O_5 glasses. *J. Non Cryst. Solids.* 463, 90–101. doi:10.1016/J.JNONCRYSOL.2017.02.022

Maddrell, E. R. (2001). Generalized titanate ceramic waste form for advanced purex reprocessing. *J. Am. Ceram. Soc.* 84, 1187–1189. doi:10.1111/j.1151-2916.2001.tb00814.x

Mahmoudysepehr, M., and Marghussian, V. K. (2009). SiO_2–PbO–CaO–ZrO_2–TiO_2–(B_2O_3–K_2O), A new zirconolite glass–ceramic system: crystallization behavior and microstructure evaluation. *J. Am. Ceram. Soc.* 92, 1540–1546. doi:10.1111/J.1551-2916.2009.03095.X

Mandal, A. K., and Sen, R. (2017). An overview on microwave processing of material: A special emphasis on glass melting. *Mater. Manuf. Process.* 32, 1–20. doi:10.1080/10426914.2016.1151046

Mandal, A., and Sen, R. (2015). Microwave absorption of barium borosilicate, zinc borate, Fe-doped alumino-phosphate glasses and its raw materials. *Technol. (Basel)* 3, 111–125. doi:10.3390/technologies3020111

Mascaraque, N., Januchta, K., Frederiksen, K. F., Youngman, R. E., Bauchy, M., and Smedskjaer, M. M. (2019). Structural dependence of chemical durability in modified aluminoborate glasses. *J. Am. Ceram. Soc.* 102, 1157–1168. doi:10.1111/jace.15969

McCloy, J. S., and Goel, A. (2017). Glass-ceramics for nuclear-waste immobilization. *MRS Bull.* 42 (3), 233–240. doi:10.1557/MRS.2017.8

Meegoda, J. N., Ezeldin, A. S., Fang, H. Y., and Inyang, H. I. (2003). Waste immobilization technologies. *Pract. Periodical Hazard. Toxic, Radioact. Waste Manag.* 7, 46–58. doi:10.1061/(ASCE)1090-025X(2003)7:1(46)

Meng, C., Li, W., Ren, C., and Zhao, J. (2020). Structure and chemical durability studies of powellite ceramics Ca1−xLix/2Gdx/2MoO4 ($0 \le x \le 1$) for radioactive waste storage. *J. Mater. Sci.* 55, 2741–2749. doi:10.1007/S10853-019-04223-Y

Mir, A. H., Hyatt, N. C., and Donnelly, S. E. (2021). An *in-situ* TEM study into the role of disorder, temperature and ballistic collisions on the accumulation of helium bubbles and voids in glass-ceramic composites. *J. Nucl. Mater.* 548, 152836. doi:10.1016/J.JNUCMAT.2021.152836

Mohapatra, M., Mishra, R. K., Kaushik, C. P., and Tomar, B. S. (2014). Investigation of radiation damage in Trombay nuclear waste glasses by ESR and photoluminescence techniques. *Procedia Mater. Sci.* 7, 247–251. doi:10.1016/j.mspro.2014.10.032

National Research Council (2011). *Waste forms technology and performance: Final report*. Washington, DC: The National Academies Press. doi:10.17226/13100

Neeway, J., Abdelouas, A., Grambow, B., and Schumacher, S. (2011). Dissolution mechanism of the SON68 reference nuclear waste glass: new data in dynamic system in silica saturation conditions. *J. Nucl. Mater.* 415, 31–37. doi:10.1016/J.JNUCMAT.2011.05.027

Neeway, J. J., Rieke, P. C., Parruzot, B. P., Ryan, J. V., and Asmussen, R. M. (2018). The dissolution behavior of borosilicate glasses in far-from equilibrium conditions. *Geochim. Cosmochim. Acta.* 226, 132–148. doi:10.1016/j.gca.2018.02.001

Nesbitt, H. W., Bancroft, G. M., Fyfe, W. S., Karkhanis, S. N., Nishijima, A., and Shin, S. (1981). Thermodynamic stability and kinetics of perovskite dissolution. *Nature* 289, 358–362. doi:10.1038/289358A0

Ojovan, M. I., and Batyukhnova, O. G. (2019). *Glasses for nuclear waste immobilization*. Tucson, AZ: WM'07 Conference.

Ojovan, M. I., Hand, R. J., Ojovan, N. V., and Lee, W. E. (2005). Corrosion of alkali–borosilicate waste glass K-26 in non-saturated conditions. *J. Nucl. Mater.* 340, 12–24. doi:10.1016/J.JNUCMAT.2004.10.095

Ojovan, M. I., Juoi, J. M., Boccaccini, A. R., and Lee, W. E. (2008). *Glass composite materials for nuclear and hazardous waste immobilisation*. Cambridge, UK: Cambridge University Press. doi:10.1557/PROC-1107-245

Ojovan, M. I., and Lee, W. E. (2014). *Immobilisation of radioactive wastes in glass, an introduction to nuclear waste immobilisation*, 245–282. doi:10.1016/B978-0-08-099392-8.00017-6

Ojovan, M. I., Lee, W. E., and Kalmykov, S. N. (2019). *An introduction to nuclear waste immobilisation*. Amsterdam, Netherlands: Elsevier.

Ojovan, M. I. (2023). Nuclear waste disposal. *Nucl. waste Dispos. Encycl.* 3 (2), 419–429. doi:10.3390/encyclopedia3020028

Ojovan, M. I., Petrov, V., and Yudintsev, S. V. (2021). Glass crystalline materials as advanced nuclear wasteforms. *Sustainability* 13 (8), 4117. doi:10.3390/su13084117

Orlova, A. I., and Ojovan, M. I. (2019). Ceramic mineral waste-forms for nuclear waste immobilization. *Mater. (Basel).* 12 (16), 2638. doi:10.3390/ma12162638

Pierce, E. M., Reed, L. R., Shaw, W. J., McGrail, B. P., Icenhower, J. P., Windisch, C. F., et al. (2010). Experimental determination of the effect of the ratio of B/Al on glass dissolution along the nepheline ($NaAlSiO_4$)–malinkoite ($NaBSiO_4$) join. *Geochim. Cosmochim. Acta.* 74 (9), 2634–2654. doi:10.1016/j.gca.2009.09.006

Pilania, R. K., Pathak, N., Saini, M., Sooraj, K. P., Ranjan, M., and Dube, C. L. (2023). Synthesis of the chemically durable glass-ceramic matrix for radioactive waste immobilisation. *Ceram. Int.* 49, 15931–15938. doi:10.1016/j.ceramint.2023.01.188

Rao, K. R. (2001). Radioactive waste: the problem and its management. *Curr. Sci. Assoc.* 81 (12), 1534–1546.

Rawlings, R. D., Wu, J. P., and Boccaccini, A. R. (2006). Glass-ceramics: their production from wastes-A review. *J. Mater. Sci.* 41, 733–761. doi:10.1007/S10853-006-6554-3

Ringwood, A. E., Kesson, S. E., Ware, N. G., Hibberson, W., and Major, A. (1979). Immobilisation of high -level nuclear reactor wastes in SYNROC. *Nature* 278, 219–223. doi:10.1038/278219a0

Ringwood, A. E. (1978). *Safe disposal of high-level nuclear reactor wastes: A new strategy*. RG Menzies: Australian National University Press.

Roessler, J. G., Townsend, T. G., and Ferraro, C. C. (2015). Use of leaching tests to quantify trace element release from waste to energy bottom ash amended pavements. *J. Hazard. Mater.* 300, 830–837. doi:10.1016/J.JHAZMAT.2015.08.028

Rossell, H. J. (1992). Solid solution of metal oxides in the zirconolite phase $CaZrTi_2O_7$. II: the ternary phase $CaZr_xTi_{3-x}O_7$. *J. solid state Chem.* 99, 52–57. doi:10.1016/0022-4596(92)90287-6

Sattonnay, G., Moll, S., Herbst-Ghysel, M., Legros, C., Costantini, J.-M., and Thomé, L. (2008). Mechanical stresses induced in ceramic oxides by ion irradiation. *Nucl. Instrum. Methods Phys. Res. B* 266 (12-13), 3052–3056. doi:10.1016/j.nimb.2008.03.162

Shamblin, J., Tracy, C. L., Ewing, R. C., Zhang, F., Li, W., Trautmann, C., et al. (2016). Structural response of titanate pyrochlores to swift heavy ion irradiation. *Acta Mater* 117, 207–215. doi:10.1016/j.actamat.2016.07.017

Shelby, J. E. (2020). *Introduction to glass science and technology*. London, UK: Royal Society of Chemistry. doi:10.1039/9781839169229

Stefanovsky, S. v., Stefanovsky, O. I., Prusakov, I. L., Kadyko, M. I., Nikonov, B. S., and Glazkova, I. S. (2019). Simulation of radioactive decay by barium substitution for cesium in sodium aluminum-iron phosphate glass. *J. Radioanal. Nucl. Chem.* 319, 817–826. doi:10.1007/s10967-018-6365-4

Stone-Weiss, N., Youngman, R. E., Thorpe, R., Smith, N. J., Pierce, E. M., and Goel, A. (2020). An insight into the corrosion of alkali aluminoborosilicate glasses in acidic environments. *Phys. Chem. Chem. Phys.* 22, 1881–1896. doi:10.1039/C9CP06064B

Strachan, D. M., Turcotte, R. P., and Barnes, B. O. (1982). MCC-1: A standard leach test for nuclear waste forms. *Nucl. Technol.* 56 (2), 306–312. doi:10.13182/NT82-A32859

Sun, K., Ding, T., Wang, L. M., and Ewing, R. C. (2003). Radiation-induced nanostructures in an iron phosphate glass. *MRS Proc.* 792, R3.21. doi:10.1557/PROC-792-R3.21

Tang, M., Kossoy, A., Jarvinen, G., Crum, J., Turo, L., Riley, B., et al. (2014). Radiation stability test on multiphase glass ceramic and crystalline ceramic waste forms. *Nucl. Instrum. Methods Phys. Res. B* 326, 293–297. doi:10.1016/J.NIMB.2013.10.092

Taylor, C. A., Patel, M. K., Aguiar, J. A., Zhang, Y., Crespillo, M. L., Wen, J., et al. (2016). Bubble formation and lattice parameter changes resulting from He irradiation of defect-fluorite $Gd_2Zr_2O_7$. *Acta Mater* 115, 115–122. doi:10.1016/j.actamat.2016.05.045

Techer, I., Advocat, T., Lancelot, J., and Liotard, J.-M. (2001). Dissolution kinetics of basaltic glasses: control by solution chemistry and protective effect of the alteration film. *Chem. Geol.* 176 (1-4), 235–263. doi:10.1016/S0009-2541(00)00400-9

Thorpe, C. L., Neeway, J. J., Pearce, C. I., Hand, R. J., Fisher, A. J., Walling, S. A., et al. (2021). Forty years of durability assessment of nuclear waste glass by standard methods. *Npj Mater. Degrad.* 5 (1), 61–28. doi:10.1038/s41529-021-00210-4

Varshneya, A. K., and Mauro, J. C. (2019). *Fundamentals of inorganic glasses, fundamentals of inorganic glasses*. Amsterdam, Netherlands: Elsevier, 1–735. doi:10.1016/C2017-0-04281-7

Wang, L., and Liang, T. (2012). Ceramics for high level radioactive waste solidification. *J. Adv. Ceram.* 1, 194–203. doi:10.1007/s40145-012-0019-8

Wang, T. T., Zhang, X. Y., Sun, M. L., Du, X., Guan, M., Peng, H. B., et al. (2020). γ-Irradiation effects in borosilicate glass studied by EPR and UV–Vis spectroscopies. *Nucl. Instrum. Methods Phys. Res. B* 464, 106–110. doi:10.1016/j.nimb.2019.12.007

Wang, X., Wu, L., Li, H., Xiao, J., Cai, X., and Teng, Y. (2017). Preparation and characterization of SO_3-doped barium borosilicate glass-ceramics containing zirconolite and barite phases. *Ceram. Int.* 43, 534–539. doi:10.1016/J.CERAMINT.2016.09.190

Weber, W. J., Ewing, R. C., Catlow, C. R. A., de la Rubia, T. D., Hobbs, L. W., Kinoshita, C., et al. (1998). Radiation effects in crystalline ceramics for the immobilization of high-level nuclear waste and plutonium. *J. Mater. Res.* 13, 1434–1484. doi:10.1557/JMR.1998.0205

Weber, W. J., Navrotsky, A., Stefanovsky, S., Vance, E. R., and Vernaz, E. (2009). Materials science of high-level nuclear waste immobilization. *MRS Bull.* 34, 46–53. doi:10.1557/mrs2009.12

Wei, G., Shu, X., Wen, M., Lu, Y., Duan, T., Chen, S., et al. (2022). Immobilization mechanism of $Gd_2Zr_2O_7$ ceramic for nuclear waste treatment. *Ceram. Int.* 48, 37164–37173. doi:10.1016/J.CERAMINT.2022.08.292

Wei, Z. J., Blackburn, L. R., Gardner, L. J., Tan, S. H., Sun, S. K., Guo, W. M., et al. (2020). Rapid synthesis of zirconolite ceramic wasteform by microwave sintering for disposition of plutonium. *J. Nucl. Mater.* 539, 152332. doi:10.1016/J.JNUCMAT.2020.152332

Wilkinson, C. J., Doss, K., Hahn, S. H., Keilbart, N., Potter, A. R., Smith, N. J., et al. (2019). Topological control of water reactivity on glass surfaces: evidence of a chemically stable intermediate phase. *J. Phys. Chem. Lett.* 10, 3955–3960. doi:10.1021/acs.jpclett.9b01275

Wu, K., Wang, F., Liao, Q., Zhu, H., Liu, D., and Zhu, Y. (2020). Synthesis of pyrochlore-borosilicate glass-ceramics for immobilization of high-level nuclear waste. *Ceram. Int.* 46, 6085–6094. doi:10.1016/j.ceramint.2019.11.071

Wu, L., Li, H., Wang, X., Xiao, J., Teng, Y., Li, Y., et al. (2016). Effects of Nd content on structure and chemical durability of zirconolite–barium borosilicate glass-ceramics. *J. Am. Ceram. Soc.* 99, 4093–4099. doi:10.1111/JACE.14440

Wu, L., Xiao, J., Wang, X., Teng, Y., Li, Y., and Liao, Q. (2018). Crystalline phase, microstructure, and aqueous stability of zirconolite–barium borosilicate glass-ceramics for immobilization of simulated sulfate bearing high-level liquid waste. *J. Nucl. Mater.* 488, 241–248. doi:10.1016/j.jnucmat.2017.10.031

Xu, H., and Wang, Y. (2000). Crystallization sequence and microstructure evolution of Synroc samples crystallized from $CaZrTi_2O_7$ melts. *J. Nucl. Mater.* 279, 100–106. doi:10.1016/S0022-3115(99)00272-X

Yang, K., Zhu, W., Scott, S., Wang, Y., Wang, J., Riley, B. J., et al. (2020). Immobilization of cesium and iodine into Cs3Bi2I9 perovskite-silica composites and core-shell waste forms with high waste loadings and chemical durability. *J. Hazard. Mater.* 401, 123279. doi:10.1016/j.jhazmat.2020.123279

Yang, R., Liu, H., Ding, Z., Zheng, J., Mauro, J. C., Kim, S. H., et al. (2021). Chemical durability of borosilicate pharmaceutical glasses: mixed alkaline earth effect with varying [MgO]/[CaO] ratio. *J. Am. Ceram. Soc.* 104, 3973–3981. doi:10.1111/jace.17850

Yang, T., Huang, X., Gao, Y., Wang, C., Zhang, Y., Xue, J., et al. (2012). Damage evolution of yttria-stabilized zirconia induced by He irradiation. *J. Nucl. Mater.* 420, 430–436. doi:10.1016/j.jnucmat.2011.10.033

Yang, T., Taylor, C. A., Wang, C., Zhang, Y., Weber, W. J., Xiao, J., et al. (2015a). Effects of He irradiation on yttria-stabilized zirconia ceramics. *J. Am. Ceram. Soc.* 98, 1314–1322. doi:10.1111/jace.13423

Yang, Y., Luo, S., Dong, F., Chen, Q., and Yang, M. (2015b). Response of strontium titanate to electron irradiation for the immobilization of strontium. *J. Radioanal. Nucl. Chem.* 303, 341–345. doi:10.1007/s10967-014-3356-y

Zanotto, E. D. (2010). A bright future for glass-ceramics. *Am. Ceram. Soc. Bull.* 89, 19–27.

Zhang, J., Wang, Y. Q., Tang, M., Sun, C., Yin, D. M., and Li, N. (2015). Helium irradiation induced micro-swelling and phase separation in pyrochlore $Lu_2Ti_2O_7$. *Nucl. Instrum. Methods Phys. Res. B* 342, 179–183. doi:10.1016/j.nimb.2014.09.036

Zhang, Y., Kong, L., Ionescu, M., and Gregg, D. J. (2022). Current advances on titanate glass-ceramic composite materials as waste forms for actinide immobilization: A technical review. *J. Eur. Ceram. Soc.* 42 (5), 1852–1876. doi:10.1016/j.jeurceramsoc.2021.12.077

Zhu, H., Wang, F., Liao, Q., Liu, D., and Zhu, Y. (2019). Structure features, crystallization kinetics and water resistance of borosilicate glasses doped with CeO_2. *J. Non Cryst. Solids.* 518, 57–65. doi:10.1016/j.jnoncrysol.2019.04.044

Zhu, H., Wang, F., Liao, Q., Wang, Y., and Zhu, Y. (2020a). Effect of CeO_2 and Nd_2O_3 on phases, microstructure and aqueous chemical durability of borosilicate glass-ceramics for nuclear waste immobilization. *Mater. Chem. Phys.* 249, 122936. doi:10.1016/J.MATCHEMPHYS.2020.122936

Zhu, H., Wang, F., Liao, Q., and Zhu, Y. (2020b). Synthesis and characterization of zirconolite-sodium borosilicate glass-ceramics for nuclear waste immobilization. *J. Nucl. Mater.* 532, 152026. doi:10.1016/J.JNUCMAT.2020.152026

Zorpette, G. (1996). Hanford's nuclear wasteland. *Hanford's Nucl. Wastel. Sci. Am.* 274 (5), 88–97. doi:10.1038/scientificamerican0596-88

Zubekhina, B. Y., Burakov, B. E., and Ojovan, M. I. (2020). Surface alteration of borosilicate and phosphate nuclear waste glasses by hydration and irradiation. *Challenges* 11 (2), 14. doi:10.3390/challe11020014